HHS Public Access

Author manuscript

Ann Neurol. Author manuscript; available in PMC 2017 November 01.

Published in final edited form as:

Ann Neurol. 2016 November ; 80(5): 776–790. doi:10.1002/ana.24791.

The neuroinflammatory component of gray matter pathology in multiple sclerosis

Elena Herranz, PhD[#1,2], **Costanza Giannì, MD**[#1,2], **Céline Louapre, MD, PhD**[1,2], **Constantina A. Treaba, MD, PhD**[1,2], **Sindhuja T. Govindarajan, MS**[1], **Russell Ouellette**[1], **Marco L Loggia, PhD**[1,2], **Jacob A. Sloane, MD**[2,3], **Nancy Madigan**[2,3], **David Izquierdo-Garcia, PhD**[1,2], **Noreen Ward, MS**[1], **Gabriel Mangeat, MS**[1,4], **Tobias Granberg, MD, PhD**[1,2], **Eric C. Klawiter, MD**[2,5], **Ciprian Catana, MD, PhD**[1,2], **Jacob M Hooker, PhD**[1,2], **Norman Taylor, MD**[2,6], **Carolina Ionete, MD, PhD**[7], **Revere P. Kinkel, MD**[3,8], and **Caterina Mainero, MD, PhD**[1,2]

[1]Athinoula A. Martinos Center for Biomedical Imaging, Department of Radiology, Massachusetts General Hospital, Boston, MA.

[2]Harvard Medical School, Boston, MA.

[3]Department of Neurology, Beth Israel Deaconess Medical Center, Boston, MA.

[4]Institute of Biomedical Engineering, Polytechnique Montréal, Montréal, QC, Canada.

[5]Department of Neurology, Massachusetts General Hospital, Boston, MA.

[6]Department of Anesthesiology, Massachusetts General Hospital, Boston, MA.

[7]UMass Multiple Sclerosis Medical Center, Worcester, MA.

[8]University of San Diego, San Diego, California.

[#] These authors contributed equally to this work.

Abstract

Objective—In multiple sclerosis (MS), using simultaneous magnetic resonance-positron emission tomography (MR-PET) imaging with ^{11}C-PBR28, we quantified expression of the 18kDa translocator protein (TSPO), a marker of activated microglia/macrophages, in cortex, cortical lesions, deep gray matter (GM), white matter (WM) lesions and normal-appearing WM (NAWM) to investigate the *in vivo* pathological and clinical relevance of neuroinflammation.

Methods—Fifteen secondary-progressive MS (SPMS) and 12 relapsing-remitting MS (RRMS) cases, and 14 matched healthy controls underwent ^{11}C-PBR28 MR-PET. MS subjects underwent 7 Tesla T_2*-weighted imaging for cortical lesions segmentation; neurological and cognitive evaluation. ^{11}C-PBR28 binding was measured using normalized 60-90-minutes standardized uptake values and volume of distribution ratios.

Corresponding author: Caterina Mainero, MD, PhD, A. A. Martinos Center for Biomedical Imaging, Building 149, Thirteenth Street, Charlestown, MA 02129, caterina@nmr.mgh.harvard.edu.

Author Contributions

Conception and design of the study: CM.

Acquisition and analysis of data: EH, CG, CL, CAT, STG, RO, ML, JAS, NM, DIG, NW, GM, TG, ECK, CC, JMH, NT, CI, RK, CM

Drafting manuscript and/or figures: EH, CG, TG, CM.

Results—Relative to controls, MS subjects exhibited abnormally high ^{11}C-PBR28 binding across the brain, the greatest increases being in cortex and cortical lesions, thalamus, hippocampus, and NAWM. MS WM lesions showed relatively modest TSPO increases. With the exception of cortical lesions, where TSPO expression was similar, ^{11}C-PBR28 uptake across the brain was greater in SPMS than in RRMS.

In MS, increased ^{11}C-PBR28 binding in cortex, deep GM, and NAWM correlated with neurological disability and impaired cognitive performance; cortical thinning correlated with increased thalamic TSPO levels.

Interpretation—In MS, neuroinflammation is present in the cortex, cortical lesions, deep GM, and NAWM, and closely linked to poor clinical outcome and, at least partly, to neurodegeneration. Distinct inflammatory-mediated factors may underlie accumulation of cortical and WM lesions. Quantification of TSPO levels in MS could prove a sensitive tool for evaluating *in vivo* the inflammatory component of GM pathology, particularly in cortical lesions.

INTRODUCTION

Demyelinated cortical lesions and diffuse cortical and deep gray matter (GM) degeneration are established components of multiple sclerosis (MS) pathology, and major substrates of disease progression[1].

The pathophysiological mechanisms leading to cortical and deep GM degeneration in MS are unknown. Early neuropathological descriptions of MS cortical lesions suggested that the histo- and immuno-pathological characteristics of cortical demyelination differ significantly from those in white matter (WM), based on the evidence that cortical lesions lacked the inflammatory pattern typical of WM plaques[2, 3]. Subsequent pathological examinations, however, suggested that cortical MS lesions might develop following meningeal inflammation accompanied by cortical microglia activation[4, 5]. The role of activated microglia in cortical MS lesion pathogenesis is not without controversies, and not uniformly observed[6]. Nevertheless, post-mortem studies demonstrate that severe cortical microglia activation and demyelination are associated with a less favorable disease outcome[4-6].

Activation of microglia/macrophages, associated with demyelination and neurodegeneration, has been pathologically observed in deep GM[7] and hippocampus in MS[8, 9], though their exact pathophysiologic role and clinical implications remain unclear.

The *in vivo* study of microglia/macrophages activation in the cortex, particularly cortical lesions, and deep GM could elucidate the role of neuroinflammation in the pathogenesis of demyelination and neurodegeneration of these structures as they usually lack the blood brain barrier abnormalities commonly detected in WM lesions using gadolinium magnetic resonance imaging (MRI)[10, 11]. Additionally, activated microglia/macrophages can be present even in the absence of the blood brain barrier disruption seen on contrast-enhanced MRI[12].

Activated microglia/macrophages upregulate expression of the 18kDa translocator protein (TSPO), which can be imaged in vivo by selective positron emission tomography (PET) TSPO radioligands, of which ^{11}C-PK11195 is the best known[13]. In MS, ^{11}C-PK11195

studies reported increased TSPO levels in the cortex[14], thalamus[15] and central deep GM[16], however, knowledge of microglia/macrophages activation in MS cortical lesions is still lacking due to the low sensitivity of clinical imaging tools to detect cortical demyelination. Seven Tesla (T) T_2*-weighted gradient-echo protocols demonstrate increased sensitivity to in vivo visualization of focal cortical lesions in MS, confirmed pathologically to correspond to cortical areas with the greatest degree of demyelination[17, 18].

^{11}C-PBR28 is a second-generation TSPO PET tracer[19] with ~80 times more specific binding than ^{11}C-PK11195[20], and good reproducibility[21]. In experimental studies inflammation-induced microglial activation determined ^{11}C-PBR28 signal increase, confirmed pathologically to mainly result from microglia binding[22].

We combined ^{11}C-PBR28 imaging on an integrated 3T magnetic resonance-positron emission tomography (MR-PET) system with 7T T_2*-weighted MRI to quantify, in a heterogeneous MS cohort, microglia/macrophages activation in the i) cortex, particularly in cortical lesions segmented at 7T; ii) thalamus, basal ganglia, and hippocampus.

We investigated the relationship between ^{11}C-PBR28 uptake in the cortex and deep GM and neurological disability, cognition, and structural MRI metrics of neurodegeneration, to better understand the prevailing effects of neuroinflammation in MS, whether mainly harmful or beneficial. Finally, we quantified ^{11}C-PBR28 uptake in lesional and normal-appearing WM (NAWM) to investigate their MRI and clinical correlates, and assess whether similar levels of TSPO expression could be detected in lesional tissue in the cortex and WM.

MATERIAL AND METHODS

Subjects

The Institutional Review Board and the Radioactive Drug Research Committee approved all study procedures, and subjects gave written informed consent to participate in the study.

Twenty-seven MS subjects (15 secondary-progressive MS, SPMS, 12 relapsingremitting MS, RRMS) were prospectively enrolled from 33 MS subjects that were genotyped for the TSPO gene Ala147Thr polymorphism, which predicts binding affinity to ^{11}C-PBR28[23]. Only high- and mixed-affinity binders underwent subsequent study procedures. Fourteen age- and TSPO affinity binding-matched healthy individuals were included as controls. Inclusion criteria were: age between 18-65 years, a diagnosis of clinically definite MS, education≥8 years, absence of clinical relapse within 3 months, no use of corticosteroids within one month of study enrollment, and being on stable disease-modifying treatment or no treatment for at least 6 months. Exclusion criteria were: treatment with benzodiazepines and blood thinners, general PET/MRI contraindications, and major medical and/or psychiatric disorders. In MS, major depression was excluded using the Beck Depression Inventory-II (cut-off score >28).

In MS subjects, within a week from imaging procedures, neurological disability was assessed using the Expanded Disability Status Scale (EDSS)[24], and cognitive performance with the following tests: Symbol Digit Modalities Test (SDMT), Trail Making Test (Trails A

and B), California Verbal Learning Test-II (CVLT-II), Brief Visuospatial Memory Test–Revised (BVMT-R) and Wisconsin Card Sorting Test–64 Card Version (WCST). For each patient, a z-score was calculated to assess information processing speed (average SDMT and Trails A z-scores), executive (average WCST and Trails B z-scores), and memory (average CVLT-II and BVMT-R z-scores) functions.

Imaging data acquisition

All subjects underwent a 90-minutes ^{11}C-PBR28 MR-PET scan on a Siemens simultaneous MR-PET system, BrainPET, a brain PET scanner operating in the bore of a 3T whole-body MR system equipped with an 8-channel head coil[25]. The spatial resolution of the BrainPET (<3 mm in the center of the field of view) is superior to that of any other whole-body PET scanner, because of the smaller size of scintillator crystals and of the scanner diameter, which minimizes the non-colinearity effect[26]. Within one week from MR-PET, 24 MS subjects underwent 7T MRI on a Siemens scanner using a 32-channel head coil. Three subjects were excluded due to the presence of implants not approved for 7T.

MR-PET acquisition—All participants received an intravenous bolus injection of ^{11}C-PBR28 produced in-house[27]. The mean±SD administrated dose was 11.4±0.7 mCi in MS and 11.7±0.5 mCi in controls. PET data were acquired in list-mode format during the 90-minutes scan. In 15 MS subjects (10 SPMS, 5 RRMS) and 11 controls, blood data were sampled from an arterial line during the 90-minutes PET acquisition (2 ml every 6 seconds during the first 3 minutes and at 5-, 10-, 20-, 30-, 60- and 90-minutes post-injection) to generate an arterial plasma input function. Plasma metabolite analysis was performed as previously outlined[28]. In the remaining subjects blood data were not collected either because they preferred not to undergo arterial line placement (N=13) or because an anesthesiologist was not available during PET (N=2).

MRI scans acquired simultaneously during PET included: a) multiple gradient echoes 3D-magnetization-prepared rapid acquisition (ME-MPRAGE) images (1 mm isotropic voxels)[29] for cortical surface reconstruction, coregistration to PET/7T data, segmentation of deep GM, generation of attenuation correction maps[30] b) conventional 3D fluid-attenuated inversion recovery (FLAIR) images (1 mm isotropic voxels) for WM lesions segmentation; c) diffusion images (60 diffusion-encoding directions, b value: 3000 s/mm^2, 8 volumes without diffusion weighting, 2.5 mm isotropic voxels) for assessing microstructural integrity in the pseudo-reference region used for normalizing PET data. In 9 patients, ME-MPRAGE and FLAIR images were acquired after administration of a single dose (0.1 mmol/kg) of gadolinium.

7T MRI acquisition—The 7T protocol included acquisition of 2D-fast low-angle shot-T_2* spoiled single- and/or multi-echo images covering the supratentorial brain (0.33×0.33×1 mm^3 voxels, 25% gap) for cortical lesions segmentation as previously detailed[18].

MRI data analysis

Lesions segmentation—White matter lesions were segmented on FLAIR images using a semi-automated method (3D-Slicer v4.2.0) and lesion volume was computed using FSL (http://fsl.fmrib.ox.ac.uk/fsl/fslwiki/FSL).

Using Slicer, 2 raters, blinded to patients' demographic/clinical data, segmented by consensus on 7T T_2*-weighted magnitude images (either from single-echo scans or, in those cases with motion artifacts in single-echo scans, from an average high-contrast image from multi-echo acquisitions) i) focal intracortical lesions and ii) leukocortical lesions, as previously detailed[18], and defined as focal cortical hyperintensities extending over at least 3 voxels across 2 consecutive slices.

No foci of enhancement were observed either in WM or GM in patients on post-gadolinium scans during MR-PET.

Cortical and subcortical gray matter segmentation—Pial and WM surfaces reconstruction and cortical thickness estimation were performed using FreeSurfer (v5.3.0, http://surfer.nmr.mgh.harvard.edu), on the 3D-ME-MPRAGE volume, the recommended anatomical sequence for FreeSurfer[29]. Topological defects in cortical surfaces due to lesions in WM and cortex were corrected with lesion in-painting.

Automated segmentation of deep GM (thalamus, hippocampus, basal ganglia) was performed using FIRST/FSL, and deep GM fractions were obtained by dividing each volume by the total intracranial volume in Freesurfer.

Diffusion imaging data—Diffusion MR images were processed using FSL/FMRIB's Diffusion Toolbox according to the following steps: 1) alignment of all images in the series to the first non-diffusion-weighted image using affine registration; 2) eddy current correction; 3) fitting of the diffusion tensor model at each voxel. Mean diffusivity maps were obtained in each subject.

Quantification of ^{11}C-PBR28 binding

In all subjects, ^{11}C-PBR28 binding was assessed across brain regions using standardized uptake values (SUV) normalized by a pseudo-reference region. In 15 MS and 11 controls, we also quantified ^{11}C-PBR28 volume of distribution (V_T) using a two-tissue compartment model with a metabolite-corrected arterial plasma curve as the input function.

^{11}C-PBR28 SUV—In-house software was used to compute voxel-wise, for each subject, SUV (mean radioactivity/injected dose/weight) from the 60-90 minutes post-injection data following a two-step process. A preliminary SUV image was created using an attenuation correction map computed from the ME-MPRAGE in its native space[30]. To account for possible motion between the time the ME-MPRAGE and the 60-90 minutes PET data were acquired, the ME-MPRAGE was coregistered to this preliminary image using SPM8. The resulting transformation matrix was applied to move the attenuation map into the final PET space. A final SUV map (sampled at 1.25 mm isotropic voxel size) was created using the new attenuation map, now well registered to the 60-90 minutes PET data. PET data were

reconstructed using 3D ordinary Poisson ordered-subset expectation maximization reconstruction, with corrections applied for attenuation, scatter, randoms, dead-time, sensitivity and normalization.

To account for global signal differences across subjects, SUV maps were normalized by a pseudo-reference region (SUVR) with mean SUV in MS around the mean of SUV in controls. Due to the fact that MS is a diffuse disease that lacks an anatomically consistent reference region, we used a cluster-based approach. Using FreeSurfer and FSL, we identified clusters (minimum size 9 contiguous voxels) in the WM of controls and NAWM of patients that were within ±0.5 SD of the mean ^{11}C-PBR28 SUV for the global WM in controls. This process was conducted separately for high- and mixed-affinity binders. In MS, NAWM was defined by subtracting WM lesions from the global WM mask. To exclude in patients the presence of microstructural changes due to inflammation[31] in the pseudo-reference region, mean diffusivity values in the selected NAWM clusters were compared to mean diffusivity values in WM clusters from controls using linear regression, and covarying for age, and no significant differences were found (MS= 6.1±0.5 10^{-10} m^2/s; controls= 6.3±0.5 10^{-10} m^2/s).

In each subject, masks of NAWM, WM lesions and deep GM were registered to SUVR maps using FNIRT/FSL to extract mean SUVR. For deep GM structures, left and right SUVR were averaged together. To minimize partial volume effects due to the thin and circumvolved nature of cortex, SUVR in the cortex and/or cortical lesions (intracortical, leukocortical) were assessed using a surface-based approach. Using Freesurfer, as previously detailed[18], in each subject, whole cortex and cortical lesions (intracortical, leukocortical) SUVR maps were registered onto their corresponding 3T cortical surface thus resulting in 2D cortical maps. Mean SUVR was computed in each map at mid-cortical depth.

^{11}C-PBR28 V_T—PET data were binned into 28 time frames (durations: 8×10, 3×20, 2×30 seconds, and 1×1, 1×2, 1×3, 8×5, 4×10 minutes), and dynamic PET images were reconstructed following the same procedure detailed above.

Plasma activity and radioactivity were fitted to a 3-exponential model to derive an input function for the radiotracer injection. The resulting metabolite-corrected plasma input function, and time-activity curves data extracted from the same regions selected for SUVR analyses were used to fit a two-tissue compartment model of radiotracer binding and calculate V_T for each region (PMOD v3.3) from the rate constant, as previously described[32, 33].

To account for i) global signal differences across subjects and ii) inter-subject variability in the input function[34], V_T were normalized by the same pseudo-reference region (DVR) used for SUV. No significant differences in V_T were found between MS subjects and controls in the pseudo-reference region.

Statistical Analysis

Statistics was performed using the R Statistics software (v2.3). Demographics and conventional MR metrics were compared in MS vs controls using Mann-Whitney-U-test. Linear regression models were used to: i) compare, in MS vs controls, SUVR and DVR

across GM (cortical lesions, whole cortex, deep GM) and WM (lesions and NAWM); ii) investigate in MS the relationship between SUVR and clinical (EDSS, cognitive scores), and structural MRI (cortical thickness, subcortical volume-fractions) metrics; iii) determine the relationship between SUVR and DVR. Age and TSPO affinity were included as covariates of no interest when appropriate. A correction for multiple comparisons was performed using the Holm method with a significance threshold of $p<0.05$ for each subset of analyses including a) SUVR and b) DVR comparisons in all MS and c-d) MS subgroups relative to controls e) correlations between SUVR and DVR, correlations between SUVR and f) EDSS, g) information processing speed and h) memory functions. The standardized effect size (Cohen's *d*) was also calculated.

Surface-based analysis—Each individual 2D-SUVR cortical map, sampled at mid-cortical depth, was smoothed along the surface with a 10 mm full-width at half-maximum Gaussian kernel and normalized to a common template in FreeSurfer. A general linear model was used to assess vertex-wise across the entire cortex: i) differences in ^{11}C-PBR28 SUVR between MS and controls, ii) the relationship in MS between ^{11}C-PBR28 SUVR and clinical scores (EDSS, cognitive scores). Binding affinity, age, and cortical thickness at the vertex level were used as covariates of no interest. Correction for multiple comparisons was performed using Monte-Carlo simulation with 10,000 iterations and a significance level of $p<0.05$. Localization of significant cortical clusters was performed using the Desikan-Killiany atlas in FreeSurfer.

RESULTS

Demographics, clinical and conventional MRI findings

Subjects' demographics, binding genotype, MRI and clinical data are reported in Table 1. Age was not statistically different between patients and controls.

Mean cortical thickness was lower in all MS and SPMS subjecys than in controls. There were no differences in deep GM fractions, only SPMS cases showed significant thalamic atrophy (Table 1).

^{11}C-PBR28 binding

TSPO levels in gray matter—Figure 1A shows ^{11}C-PBR28 SUVR distribution across brain regions in controls and MS subjects, according to their binding genotype. DVR comparisons between MS and controls are illustrated in Figure 1B. Table 2 reports significant differences between groups, and their effect size. Relative to controls, MS cases showed increased ^{11}C-PBR28 SUVR in the whole cortex (23%) thalamus (50%,), hippocampus (28%) and basal ganglia (26%). Thalamic lesions were observed in 12 patients (9 SPMS, 3 RRMS) but not in other deep GM structures. Thalamic lesions' SUVR did not differ from uptake in normal appearing thalamus (paired t-test).

Twenty MS subjects (SPMS=12, RRMS=8) had visible cortical lesions on 7T scans (Table 1). In 2 patients no cortical lesions could be detected, while in 2 participants 7T images were discarded due to gross motion artifacts. Relative to controls' cortex, ^{11}C-PBR28 SUVR were increased by 28% in intracortical lesions and by 24% in leukocortical lesions. Increased ^{11}C-

PBR28 uptake in cortical lesions did not differ significantly from that in normal appearing cortex (paired t-test).

The ^{11}C-PBR28 DVR were significantly increased in MS (n=15) relative to controls (n=11) in the whole cortex (30%), thalamus (44%), hippocampus (25%), and basal ganglia (19%), (Fig 1B, Table 2). Cortical lesions DVR were also significantly increased (29%) relative to controls' cortex in MS patients (n=9). Due to the small number of cases with both cortical lesions and blood data, cortical lesions DVR were assessed by grouping intracortical and leukocortical lesions.

Figure 2 illustrates examples of MS cortical lesions on 7T scans that co-localized with areas of increased ^{11}C-PBR28 uptake on fused MR-PET images, and of diffuse thalamic increased tracer binding in MS.

TSPO levels in white matter—Higher TSPO levels were found in MS NAWM relative to controls WM (Fig 1A to B, Table 2), with a 20% increase in SUVR, and a 29% increase in DVR. For WM lesions, we found a modest increase (7%) in ^{11}C-PBR28 SUVR, while higher TSPO levels could be detected in ^{11}C-PBR28 DVR (15%).

TSPO levels in RRMS and SPMS—Corrected p-values and effect size for comparisons of ^{11}C-PBR28 SUVR and DVR in each MS subgroup relative to controls are reported in Table 2. RRMS showed significant ^{11}C-PBR28 increases in intracortical lesions and whole cortex. SUVR were also increased in thalamus, and hippocampus by ~29-22% though at an uncorrected significance level. SPMS showed significantly increased SUVR and DVR in the whole cortex (28%, 32%), cortical lesions (ranging from 24% to 36%), thalamus (64%, 58%), hippocampus (33%, 30%), and basal ganglia (34%, 25%). SUVR and DVR were increased by 27% and 32% in NAWM. Increased ^{11}C-PBR28 uptake in WM lesions was significant only for DVR (21%).

Association between SUVR and DVR throughout the brain—In all 15 MS subjects (7 with high- and 8 with mixed-affinity binding) and in 11 controls (5 with high- and 6 with mixed-affinity binding) with blood data there was a positive correlation between SUVR and DVR across all brain tissue compartments (Fig 3).

Correlation with clinical and structural MRI data

In the MS cohort, EDSS correlated positively with increased ^{11}C-PBR28 SUVR in the whole cortex, thalamus, hippocampus, and basal ganglia. A positive association was also found with ^{11}C-PBR28 uptake in the NAWM and WM lesions (Fig 4).

Impaired memory function scores were associated with increased TSPO levels in the thalamus, while we did not find any association with information processing speed function obtained by averaging SDMT and Trails A scores. Looking at individual tests we found that SDMT z-scores negatively correlated with ^{11}C-PBR28 SUVR in thalamus, hippocampus and NAWM (Fig 4). There was no association between ^{11}C-PBR28 uptake and executive function.

In all patients and in each MS subgroup, cortical thinning was associated with increased TSPO levels in the thalamus ($p<0.05$ corrected, covarying for age, binding affinity). In SPMS only, cortical thinning also correlated with neuroinflammation in the cortex and NAWM, though at an uncorrected significance level.

Surface-based analysis of cortical ^{11}C-PBR28 binding

The cortical surface-based analysis revealed several clusters of increased ^{11}C-PBR28 SUVR in both hemispheres in the entire MS cohort vs controls (Fig 5 A to C, Table 3). The increase in ^{11}C-PBR28 cortical uptake was diffuse in SPMS, while more localized in RRMS.

Negative correlations were detected between information processing speed and memory function and ^{11}C-PBR28 uptake in widespread fronto-parietal, temporal and occipital regions, and right cingulate cortex (Fig 5 D to E, Table 3).

No vertex-wise associations were found with executive function or EDSS.

DISCUSSION

Using ^{11}C-PBR28, a second-generation TSPO radiotracer, we demonstrated diffuse microglia/macrophages activation in the cortex, including cortical lesions, and deep GM of MS cases.

Cortical demyelination is a well-established neuropathological feature of MS, and a main substrate of disease progression[2, 4]. In histopathological examinations, cortical lesions, particularly in progressive MS, usually lacked the typical inflammatory features of WM plaques[2, 3], and activated microglia was the prominent cellular population[2, 4].

We used a surface-based analysis to assess, in MS relative to controls, either in cortical lesions imaged with ultra-high resolution 7T MRI, or, vertex-wise across the whole cortex, differences in TSPO expression sampled at mid-cortical depth. Compared to volumetric approaches, this method has been shown to improve reliability and detectability of PET cortical signal changes[35]. A previous ^{11}C-PK11195 PET data, using a volume of interest approach, showed increased TSPO levels in MS in frontal, parietal and occipital cortices[14]. Here, we found that all MS disease stages exhibited abnormally increased TSPO levels, indicative of microglia/macrophages activation, in cortical lesions and several areas of the cortical ribbon. The highest concentration of cortical microglia/macrophages activation was localized in the occipital and temporal cortex in RRMS, the latter often reported as preferential location for cortical MS demyelination[36], while it extended to widespread frontal and parietal regions in SPMS.

In some neuropathological studies of progressive MS, cortical lesions appeared topographically associated with meningeal inflammatory infiltrates, leading to the hypothesis that cortical demyelination may be induced by soluble factors, which diffuse from the meninges into the cortex and trigger demyelination directly or indirectly through microglia activation[5, 37]. The extent of meningeal inflammation correlated with microglia activation and the severity of demyelination in the underlying cortex[4, 5]. Meningeal inflammation, by means of perivascular lymphocytic infiltration, in association with cortical

lesions, has also been described in biopsies at MS onset[37]. The possibility to quantify in vivo TSPO levels in cortical lesions could provide a tool for assessing the innate immune system inflammatory component of cortical lesions, its severity and association to structural cortical integrity. Additionally, it could offer relevant information on the role of microglia/macrophages activation in cortical lesions development at any disease stage. Interestingly, in contrast to WM plaques, RRMS and SPMS showed similarly increased TSPO levels in cortical lesions.

Histopathological findings on the role of inflammation in subcortical GM demyelination and neurodegeneration in MS are sparse and heterogeneous, and variable degrees of inflammation by means of activated microglia/macrophages have been reported in deep GM[7, 38] and hippocampus[7, 9]. In this study, we showed that microglia/macrophages activation extensively involved the thalamus, hippocampus and basal ganglia. Previous ^{11}C-PK11195 PET studies reported increased thalamic TSPO levels in MS[13, 15]. Abnormally high ^{11}C-PK11195 binding has also been observed in clinically isolated syndrome in the brain central deep GM, though no significant differences were found in any single deep GM structure relative to controls[39]. Here, neuroinflammation in thalamus and deep GM was seen at both disease stages though more prominently in SPMS.

Our MS cohort showed, relative to controls, significant global cortical thinning, while there were no differences in deep GM volumes with the exception of thalamic atrophy in SPMS. Cortical thinning in MS correlated with increased thalamic ^{11}C-PBR28 binding. Increased thalamic ^{11}C-PK11195 uptake secondary to distant cortical pathology has been described in stroke[40], implying the existence of a “projected neuroinflammatory” response from distant lesions along shared anatomical pathways. The thalami are major hubs in the brain, which integrate and process the signal originating from cortical projections. Spreading of cortical pathology to the thalami, or viceversa, could occur through thalamo-cortical connections. The direction of such changes could be tested in MS by assessing, longitudinally, microglia/macrophages activation changes along cortico-thalamic pathways.

The exact relationship between cortical neurodegeneration and locally activated microglia needs to be elucidated. Pathological evidence suggested that, as for cortical lesions development, neurodegeneration may be triggered by meningeal inflammation with cortical microglia activation[4, 5, 37]. In a series of RRMS and SPMS cases, leptomeningeal inflammation, as seen on post-contrast FLAIR MRI, was found to be associated with more severe cortical atrophy[41]. According to some experimental studies microglial activation may also constitute a specialized danger signal following neuronal death or injury[42]. In our cohort, however, especially in RRMS, neuroinflammation was, was not strictly associated with neurodegeneration suggesting that it might not simply represent an indirect marker or consequence of neuroaxonal loss.

In line with previous observations, we found increased TSPO levels in WM lesions[43, 44] and NAWM[16, 43, 45]. We found that TPSO levels in WM lesions, measured with both SUVR and DVR, were generally lower than those in cortical lesions. Additionally, in RRMS, the highest ^{11}C-PBR28 uptake, relative to controls, was measured in intracortical lesions and focal cortical areas, while it was relatively modest in WM. Overall, these observations

suggest that the innate immune system-mediated inflammatory events underlying the development of MS lesions might be dissociated in cortex and WM, especially in earlier disease stages, or there may be more heterogeneity in the inflammatory response associated with WM plaques[46] than with cortical lesions. It is possible, however, that even if 7T MRI was used for cortical lesions detection, some cortical lesions were missed at visual inspection of scans. Nevertheless, cortical lesions identified on 7T T_2*-weighted images likely represent the areas with greatest cortical demyelination, especially in RRMS[18].

In our MS cohort, neurological disability correlated with microglial/macrophages activation in deep GM, in addition to neuroinflammation in the cortex and WM as previously reported[14, 16]. Here, we also demonstrated that microglia/macrophages activation correlated with reduced cognitive performance in MS. Increased TSPO levels in thalamus, hippocampus, and NAWM were associated with impaired SDMT function, a measure of information processing speed, which is frequently affected in MS and, thus, commonly evaluated in clinical setting. Diffusion imaging data highlighted that hippocampal-thalamic-prefrontal disruption affects SDMT performance in RRMS[47]. An association between depression and hippocampal neuroinflammation, as measured ^{18}F-PBR11, has been recently reported in RRMS[39]. Our study excluded cases with major depression or other psychiatric conditions, and moderate depression was present only in 3 MS patients. Interestingly, in our cohort, information processing speed dysfunction also correlated with increased ^{11}C-PBR28 binding in fronto-parietal, temporal, cingulate, and occipital cortices, in line with previous functional MRI experiments that described large areas of activation in the same cortical regions during SDMT execution[48]. Finally, neuroinflammation in the thalamus, and in widespread temporal and occipital regions, and extending to the cingulate and prefrontal cortex, was associated with decreased memory function as measured by the BVMT-R and CVLT-II likely reflecting the different neuroanatomical correlates for memory processing of verbal and visual material.

It has been hypothesized that microglia may play a dual role in MS pathogenesis: either detrimental, by causing neuronal dysfunction and promoting oxidative burst, or neuroprotective. Our findings suggest that the prevailing effects, both in GM and NAWM, are detrimental. The observation that SPMS cases showed overall higher brain TSPO levels than RRMS cases further supports this notion. It cannot be excluded, however that, at least in early disease stages, microglia might exert protective functions. Recent data, however, demonstrated that in clinically isolated syndrome persistently increased TSPO levels in NAWM predicted conversion to MS[16].

We assessed TSPO levels using ^{11}C-PBR28 SUVR and quantitative blood analysis, with both measures showing similar changes in MS. As previously suggested[34], we used DVR to account for ^{11}C-PBR28 inter-subject variability in the input function. Our and previous ^{11}C-PBR28 data[21] seem to suggest that quantitative blood data may be more sensitive than SUVR to microglia/macrophages activation in MS WM lesions, though this needs to be further confirmed. However, the strong, positive correlation between SUVR and DVR in all tissue compartments assessed indicates that SUVR estimation is a reliable method for characterizing microglial/macrophages pathology in MS. In humans, ^{11}C-PBR28 SUVR have also been used to reliably distinguish healthy individuals from cases with neurological

disorders[27, 49, 50]. This method is expected to improve subject tolerability by allowing shorter scan time and not requiring arterial catheterization, making it less invasive and more feasible for clinical studies. The use of an integrated MR-PET system further increases patients' compliance, in addition to improving spatial fidelity and registration accuracy[25].

In this study, we could assess blood brain barrier integrity with contrast-enhanced MRI only in a third of MS subjects, thus we cannot definitely exclude that some of the TSPO changes in the remaining patients were secondary to acute systemic inflammation. However, blood brain barrier disruption in cortex and deep GM is uncommonly observed in MS using contrast-enhanced MRI[10,11], and all patients were stable in terms of clinical relapses and MS-related treatments, suggesting that microglia/macrophages activation likely, largely reflected chronic inflammation, especially in SPMS.

Microglia could constitute a potential target for monitoring disease course, especially in the compartmentalized inflammation in progressive MS, and the effects of therapies. Our findings could guide longitudinal evaluations in larger MS cohorts to definitely establish the role of neuroinflammation in disease pathogenesis and progression.

Acknowledgments

This study was supported partly by the Clafin Award; partly by a grant from the National MS Society (NMSS) RG 4729A2/1, and partly by the Department of Defense (DoD) US Army W81XWH-13-1-0112 Award. Elena Herranz was supported by an NMSS fellowship FG-1507-05459. Céline Louapre was supported by a fellowship from ARSEP foundation. Costanza Giannì was supported by FISM training fellowship 2012/B/04. Marco Loggia was supported by NIH 1R21NS087472-01A1

DoD W81XWH-14-1-0543.

We would like to thank Grae Arabasz, Shirley Hsu and Marlene Wentworth for their technical and medical assistance with the MR-PET imaging; Federico Turkheimer, Mattia Veronese and Daniel A. Albrecht for their help with quality control of the blood data.

REFERENCES

1. Zivadinov R, Pirko I. Advances in understanding gray matter pathology in multiple sclerosis: are we ready to redefine disease pathogenesis? BMC Neurol. 2012; 12:9. [PubMed: 22394621]
2. Peterson JW, Bo L, Mork S, Chang A, Trapp BD. Transected neurites, apoptotic neurons, and reduced inflammation in cortical multiple sclerosis lesions. Ann Neurol. Sep; 2001 50(3):389–400. [PubMed: 11558796]
3. Bo L, Vedeler CA, Nyland H, Trapp BD, Mork SJ. Intracortical multiple sclerosis lesions are not associated with increased lymphocyte infiltration. Mult Scler. Aug; 2003 9(4):323–31. [PubMed: 12926836]
4. Magliozzi R, Howell O, Vora A, et al. Meningeal B-cell follicles in secondary progressive multiple sclerosis associate with early onset of disease and severe cortical pathology. Brain. Apr; 2007 130(Pt 4):1089–104. [PubMed: 17438020]
5. Howell OW, Reeves CA, Nicholas R, et al. Meningeal inflammation is widespread and linked to cortical pathology in multiple sclerosis. Brain. Sep; 2011 134(Pt 9):2755–71. [PubMed: 21840891]
6. Kooi EJ, Strijbis EM, van der Valk P, Geurts JJ. Heterogeneity of cortical lesions in multiple sclerosis: clinical and pathologic implications. Neurology. Sep 25; 2012 79(13):1369–76. [PubMed: 22972651]
7. Haider L, Simeonidou C, Steinberger G, et al. Multiple sclerosis deep grey matter: the relation between demyelination, neurodegeneration, inflammation and iron. J Neurol Neurosurg Psychiatry. Dec; 2014 85(12):1386–95. [PubMed: 24899728]

8. Geurts JJ, Bo L, Roosendaal SD, et al. Extensive hippocampal demyelination in multiple sclerosis. J Neuropathol Exp Neurol. Sep; 2007 66(9):819–27. [PubMed: 17805012]
9. Dutta R, Chang A, Doud MK, et al. Demyelination causes synaptic alterations in hippocampi from multiple sclerosis patients. Ann Neurol. Mar; 2011 69(3):445–54. [PubMed: 21446020]
10. Calabrese M, Filippi M, Rovaris M, et al. Morphology and evolution of cortical lesions in multiple sclerosis. A longitudinal MRI study. Neuroimage. Oct 1; 2008 42(4):1324–8. [PubMed: 18652903]
11. Renard D, Castelnovo G, Campello C, et al. Thalamic lesions: a radiological review. Behav Neurol. 2014; 2014:154631. [PubMed: 25100900]
12. Oh U, Fujita M, Ikonomidou VN, et al. Translocator protein PET imaging for glial activation in multiple sclerosis. J Neuroimmune Pharmacol. Sep; 6(3):354–61. [PubMed: 20872081]
13. Banati RB, Newcombe J, Gunn RN, et al. The peripheral benzodiazepine binding site in the brain in multiple sclerosis: quantitative in vivo imaging of microglia as a measure of disease activity. Brain. Nov; 2000 123(Pt 11):2321–37. [PubMed: 11050032]
14. Politis M, Giannetti P, Su P, et al. Increased PK11195 PET binding in the cortex of patients with MS correlates with disability. Neurology. Aug 7; 2012 79(6):523–30. [PubMed: 22764258]
15. Rissanen E, Tuisku J, Rokka J, et al. In Vivo Detection of Diffuse Inflammation in Secondary Progressive Multiple Sclerosis Using PET Imaging and the Radioligand (1)(1)C-PK11195. J Nucl Med. Jun; 2014 55(6):939–44. [PubMed: 24711650]
16. Giannetti P, Politis M, Su P, et al. Increased PK11195-PET binding in normal-appearing white matter in clinically isolated syndrome. Brain. Jan; 2015 138(Pt 1):110–9. [PubMed: 25416179]
17. Filippi M, Evangelou N, Kangarlu A, et al. Ultra-high-field MR imaging in multiple sclerosis. J Neurol Neurosurg Psychiatry. Jan; 2014 85(1):60–6. [PubMed: 23813636]
18. Louapre C, Govindarajan ST, Gianni C, et al. Beyond focal cortical lesions in MS: An in vivo quantitative and spatial imaging study at 7T. Neurology. Nov 10; 2015 85(19):1702–9. [PubMed: 26468411]
19. Brown AK, Fujita M, Fujimura Y, et al. Radiation dosimetry and biodistribution in monkey and man of 11C-PBR28: a PET radioligand to image inflammation. J Nucl Med. Dec; 2007 48(12): 2072–9. [PubMed: 18006619]
20. Kreisl WC, Fujita M, Fujimura Y, et al. Comparison of [(11)C]-(R)-PK 11195 and [(11)C]PBR28, two radioligands for translocator protein (18 kDa) in human and monkey: Implications for positron emission tomographic imaging of this inflammation biomarker. Neuroimage. Feb 15; 2010 49(4): 2924–32. [PubMed: 19948230]
21. Park E, Gallezot JD, Delgadillo A, et al. (11)C-PBR28 imaging in multiple sclerosis patients and healthy controls: test-retest reproducibility and focal visualization of active white matter areas. Eur J Nucl Med Mol Imaging. Jun; 2015 42(7):1081–92. [PubMed: 25833352]
22. Hannestad J, Gallezot JD, Schafbauer T, et al. Endotoxin-induced systemic inflammation activates microglia: [(1)(1)C]PBR28 positron emission tomography in nonhuman primates. Neuroimage. Oct 15; 2012 63(1):232–9. [PubMed: 22776451]
23. Owen DR, Yeo AJ, Gunn RN, et al. An 18-kDa translocator protein (TSPO) polymorphism explains differences in binding affinity of the PET radioligand PBR28. J Cereb Blood Flow Metab. Jan; 2012 32(1):1–5. [PubMed: 22008728]
24. Kurtzke JF. Rating neurologic impairment in multiple sclerosis: an expanded disability status scale (EDSS). Neurology. Nov; 1983 33(11):1444–52. [PubMed: 6685237]
25. Catana C, van der Kouwe A, Benner T, et al. Toward implementing an MRI-based PET attenuation-correction method for neurologic studies on the MR-PET brain prototype. J Nucl Med. Sep; 2010 51(9):1431–8. [PubMed: 20810759]
26. Kolb A, Wehrl HF, Hofmann M, et al. Technical performance evaluation of a human brain PET/MRI system. Eur Radiol. Aug; 2012 22(8):1776–88. [PubMed: 22752524]
27. Zurcher NR, Loggia ML, Lawson R, et al. Increased in vivo glial activation in patients with amyotrophic lateral sclerosis: assessed with [(11)C]-PBR28. Neuroimage Clin. 2015; 7:409–14. [PubMed: 25685708]

28. Granda ML, Schroeder FA, Borra RH, et al. First D1-like receptor PET imaging of the rat and primate kidney: implications for human disease monitoring. Am J Physiol Renal Physiol. Jul 1; 2014 307(1):F116–21. [PubMed: 24808534]
29. van der Kouwe AJ, Benner T, Salat DH, Fischl B. Brain morphometry with multiecho MPRAGE. Neuroimage. Apr 1; 2008 40(2):559–69. [PubMed: 18242102]
30. Izquierdo-Garcia D, Hansen AE, Forster S, et al. An SPM8-based approach for attenuation correction combining segmentation and nonrigid template formation: application to simultaneous PET/MR brain imaging. J Nucl Med. Nov; 2014 55(11):1825–30. [PubMed: 25278515]
31. Liu Y, Mitchell PJ, Kilpatrick TJ, et al. Diffusion tensor imaging of acute inflammatory lesion evolution in multiple sclerosis. J Clin Neurosci. Dec; 2012 19(12):1689–94. [PubMed: 23084347]
32. Gunn RN, Lammertsma AA, Grasby PM. Quantitative analysis of [carbonyl-(11)C]WAY-100635 PET studies. Nucl Med Biol. Jul; 2000 27(5):477–82. [PubMed: 10962254]
33. Fujita M, Imaizumi M, Zoghbi SS, et al. Kinetic analysis in healthy humans of a novel positron emission tomography radioligand to image the peripheral benzodiazepine receptor, a potential biomarker for inflammation. Neuroimage. Mar 1; 2008 40(1):43–52. [PubMed: 18093844]
34. Turkheimer FE, Rizzo G, Bloomfield PS, et al. The methodology of TSPO imaging with positron emission tomography. Biochem Soc Trans. Aug 1; 2015 43(4):586–92. [PubMed: 26551697]
35. Greve DN, Svarer C, Fisher PM, et al. Cortical surface-based analysis reduces bias and variance in kinetic modeling of brain PET data. Neuroimage. May 15.2014 92:225–36. [PubMed: 24361666]
36. Bo L, Vedeler CA, Nyland HI, Trapp BD, Mork SJ. Subpial demyelination in the cerebral cortex of multiple sclerosis patients. J Neuropathol Exp Neurol. Jul; 2003 62(7):723–32. [PubMed: 12901699]
37. Lucchinetti CF, Popescu BF, Bunyan RF, et al. Inflammatory cortical demyelination in early multiple sclerosis. N Engl J Med. Dec 8; 2011 365(23):2188–97. [PubMed: 22150037]
38. Vercellino M, Masera S, Lorenzatti M, et al. Demyelination, inflammation, and neurodegeneration in multiple sclerosis deep gray matter. J Neuropathol Exp Neurol. May; 2009 68(5):489–502. [PubMed: 19525897]
39. Colasanti A, Guo Q, Giannetti P, et al. Hippocampal Neuroinflammation, Functional Connectivity, and Depressive Symptoms in Multiple Sclerosis. Biol Psychiatry. Dec 5.2015
40. Pappata S, Levasseur M, Gunn RN, et al. Thalamic microglial activation in ischemic stroke detected in vivo by PET and [11C]PK1195. Neurology. Oct 10; 2000 55(7):1052–4. [PubMed: 11061271]
41. Absinta M, Vuolo L, Rao A, et al. Gadolinium-based MRI characterization of leptomeningeal inflammation in multiple sclerosis. Neurology. Jul 7; 2015 85(1):18–28. [PubMed: 25888557]
42. Hanisch UK, Kettenmann H. Microglia: active sensor and versatile effector cells in the normal and pathologic brain. Nat Neurosci. Nov; 2007 10(11):1387–94. [PubMed: 17965659]
43. Colasanti A, Guo Q, Muhlert N, et al. In Vivo Assessment of Brain White Matter Inflammation in Multiple Sclerosis with (18)F-PBR111 PET. J Nucl Med. Jul; 2014 55(7):1112–8. [PubMed: 24904112]
44. Oh U, Fujita M, Ikonomidou VN, et al. Translocator protein PET imaging for glial activation in multiple sclerosis. J Neuroimmune Pharmacol. Sep; 2011 6(3):354–61. [PubMed: 20872081]
45. Debruyne JC, Versijpt J, Van Laere KJ, et al. PET visualization of microglia in multiple sclerosis patients using [11C]PK11195. Eur J Neurol. May; 2003 10(3):257–64. [PubMed: 12752399]
46. Lucchinetti C, Bruck W, Parisi J, Scheithauer B, Rodriguez M, Lassmann H. Heterogeneity of multiple sclerosis lesions: implications for the pathogenesis of demyelination. Ann Neurol. Jun; 2000 47(6):707–17. [PubMed: 10852536]
47. Kern KC, Gold SM, Lee B, et al. Thalamic-hippocampal-prefrontal disruption in relapsing-remitting multiple sclerosis. Neuroimage Clin. 2015; 8:440–7. [PubMed: 26106524]
48. Forn C, Belenguer A, Belloch V, Sanjuan A, Parcet MA, Avila C. Anatomical and functional differences between the Paced Auditory Serial Addition Test and the Symbol Digit Modalities Test. J Clin Exp Neuropsychol. Jan; 2011 33(1):42–50. [PubMed: 20552497]
49. Lyoo CH, Ikawa M, Liow JS, et al. Cerebellum Can Serve As a Pseudo-Reference Region in Alzheimer Disease to Detect Neuroinflammation Measured with PET Radioligand Binding to Translocator Protein. J Nucl Med. May; 2015 56(5):701–6. [PubMed: 25766898]

50. Loggia ML, Chonde DB, Akeju O, et al. Evidence for brain glial activation in chronic pain patients. Brain. Mar; 2015 138(Pt 3):604–15. [PubMed: 25582579]

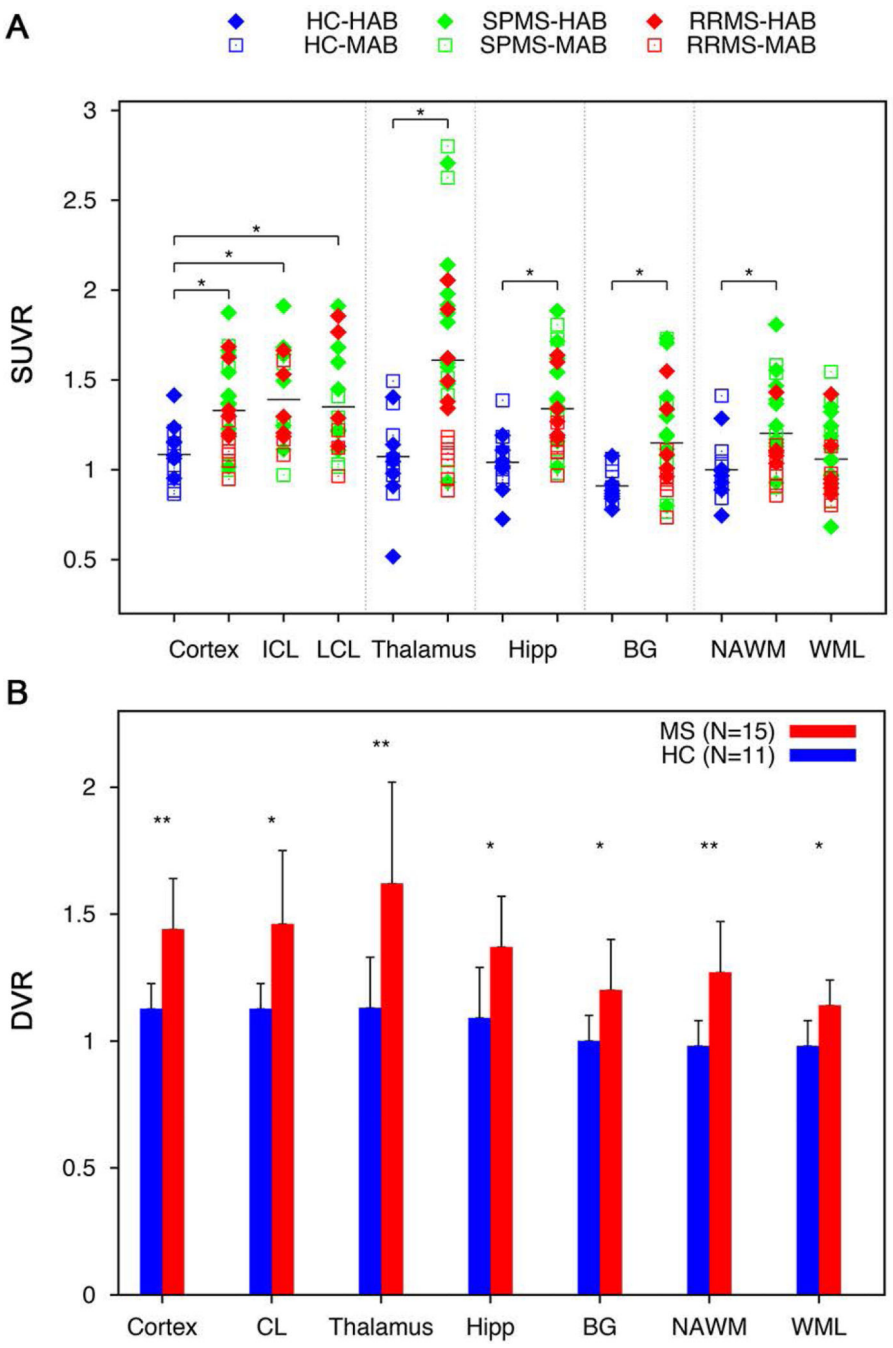

Figure 1.

A) Mean normalized ^{11}C-PBR28 standardized uptake values (SUVR) in healthy controls (n=14) and patients (n=27) with either relapsing-remitting or secondary-progressive multiple sclerosis (RRMS, n=12; SPMS, n=15) across different tissue compartments in gray and white matter. Horizontal bars indicate group averages for HAB= high-affinity binder, MAB= mixed-affinity binder. Connector-lines connect brain tissue compartments that were compared in the whole MS cohort relative to controls using linear regression and covarying for age and affinity binding. In MS, mean SUVR in intracortical and leukocortical lesions

were compared with mean cortical SUVR from controls. The asterisks denote when the specific comparison, connector-line, between healthy controls and MS patients was statistically significant.

B) Histogram showing mean ^{11}C-PBR28 normalized volume of distributions (DVR) and standard deviations in different brain regions for both multiple sclerosis (MS) subjects (n=15) and controls (n=11). ^{11}C-PBR28 DVR were significantly increased in MS subjects compared to controls in all regions assessed. DVR cortical lesions analysis was performed in 9 MS patients.

*p<0.05, **p<0.005, by linear regression, adjusting for binding genotype and age, and corrected for multiple comparisons. HC= healthy controls; HAB= high affinity binder; MAB= mixed affinity binder; ICL= intracortical lesions; LCL= leukocortical lesions; Hipp= hippocampus; BG= basal ganglia; NAWM= normal appearing white matter; WML= white matter lesions; CL= cortical lesions.

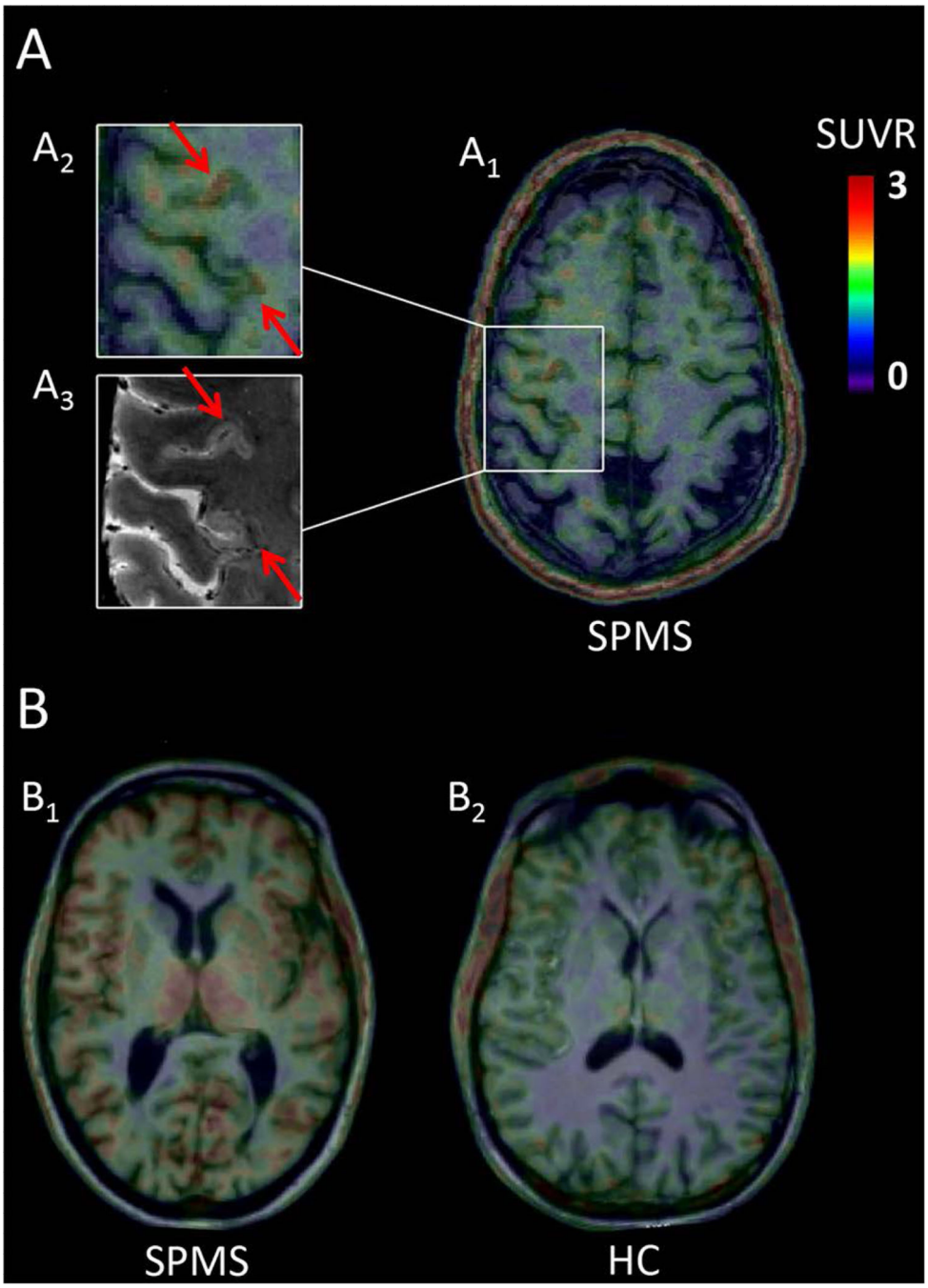

Figure 2.

A) Fused magnetic resonance and positron emission tomography (MR-PET) images in a subject with secondary-progressive multiple sclerosis (SPMS) and a high affinity binding (HAB) genotype **(A_1)** showing cortical areas of increased ^{11}C-PBR28 standardized uptake values normalized by a pseudo-reference region (SUVR). **(A_2)** Detail of cortical lesions visible on the 3 Tesla (T) anatomical scan fused with SUVR images and **(A_3)** on the co-registered 7T T_2* images. **B)** Fused ^{11}C-PBR28 SUVR MR-PET images in a HAB MS

subject **(B_1)** and in a HAB age-matched healthy control (**B_2**) showing increased ^{11}C-PBR28 SUVR uptake in the thalamus of the patient.

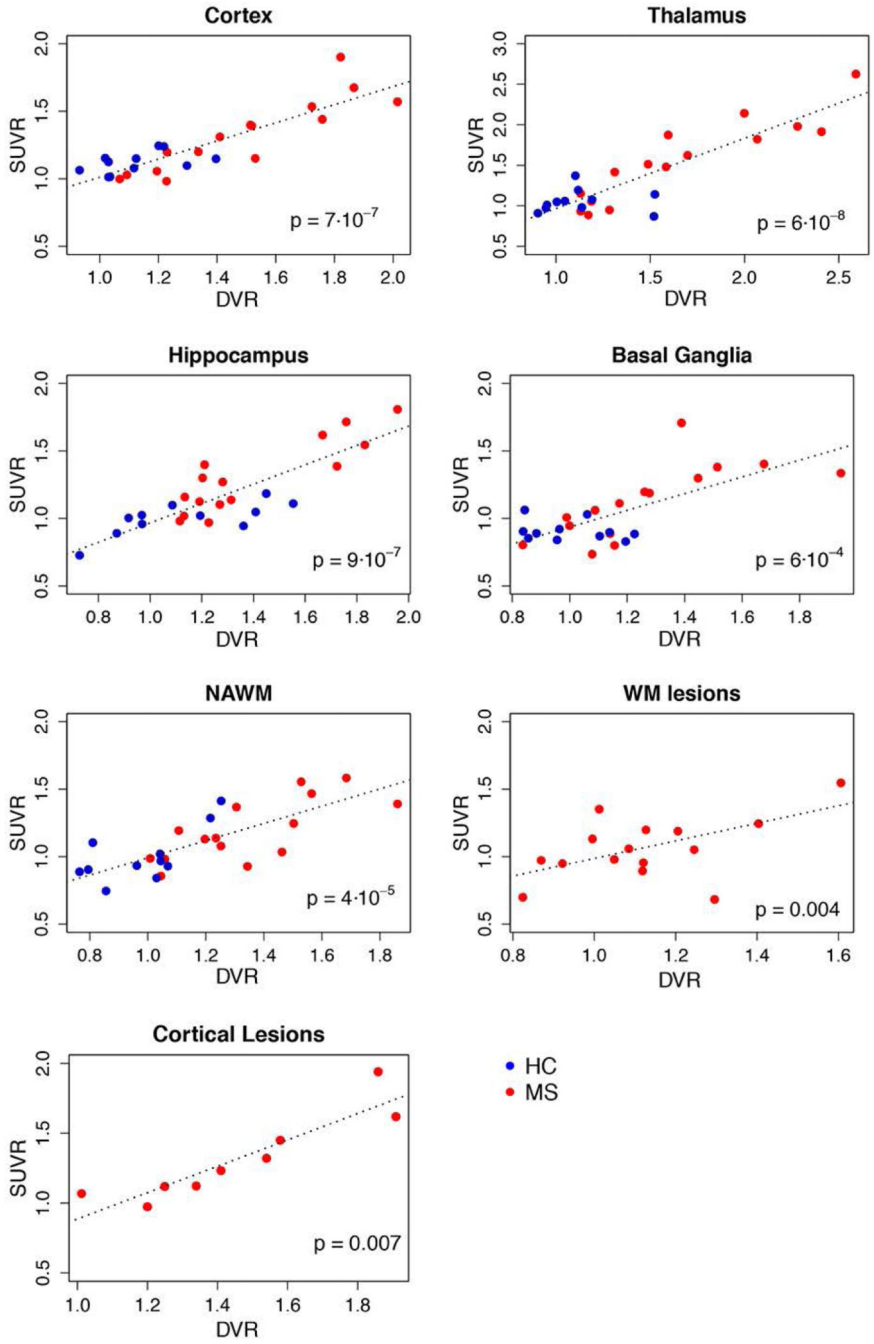

Figure 3.

Plots illustrating, in the whole study cohort, the correlation between ^{11}C-PBR28 normalized volume of distributions (DVR) and standardized uptake values (SUVR) across different brain tissue compartments by linear regression, adjusting for binding genotype and correcting for multiple comparisons. HC= healthy controls; MS= multiple sclerosis; NAWM= normal-appearing white matter; WM= white matter.

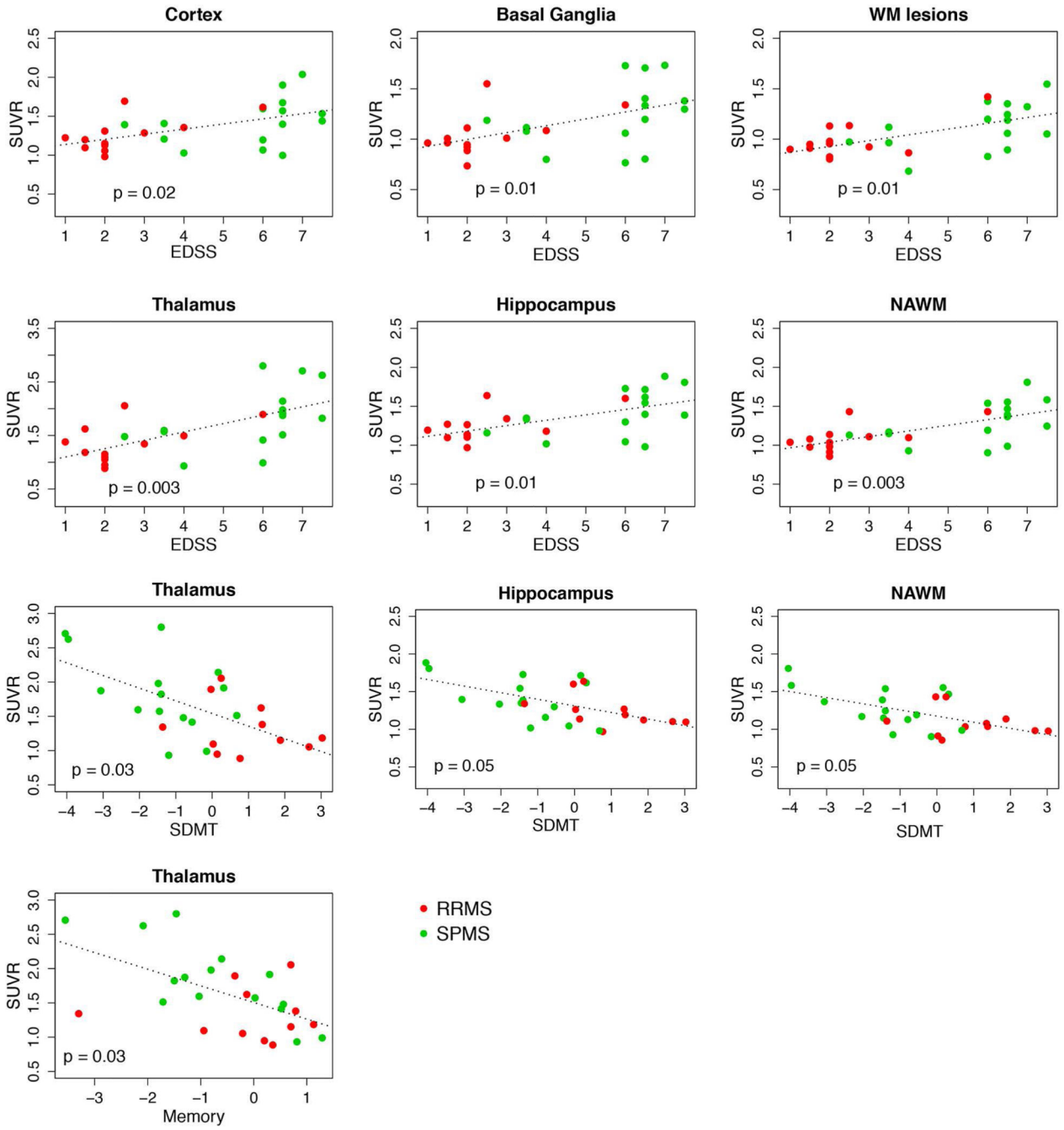

Figure 4.

Plots illustrating, in the whole multiple sclerosis (MS) cohort, correlations between ^{11}C-PBR28 normalized standardized uptake values (SUVR) and neurological disability and cognitive test scores (linear regression analysis, adjusting for binding genotype, age. All p values are corrected for multiple comparisons). EDSS= Expanded Disability Status Scale; NAWM= normal-appearing white matter; WM= white matter; SDMT= Symbol Digit Modalities Test, RRMS= relapsing-remitting MS; SPMS= secondary-progressive MS.

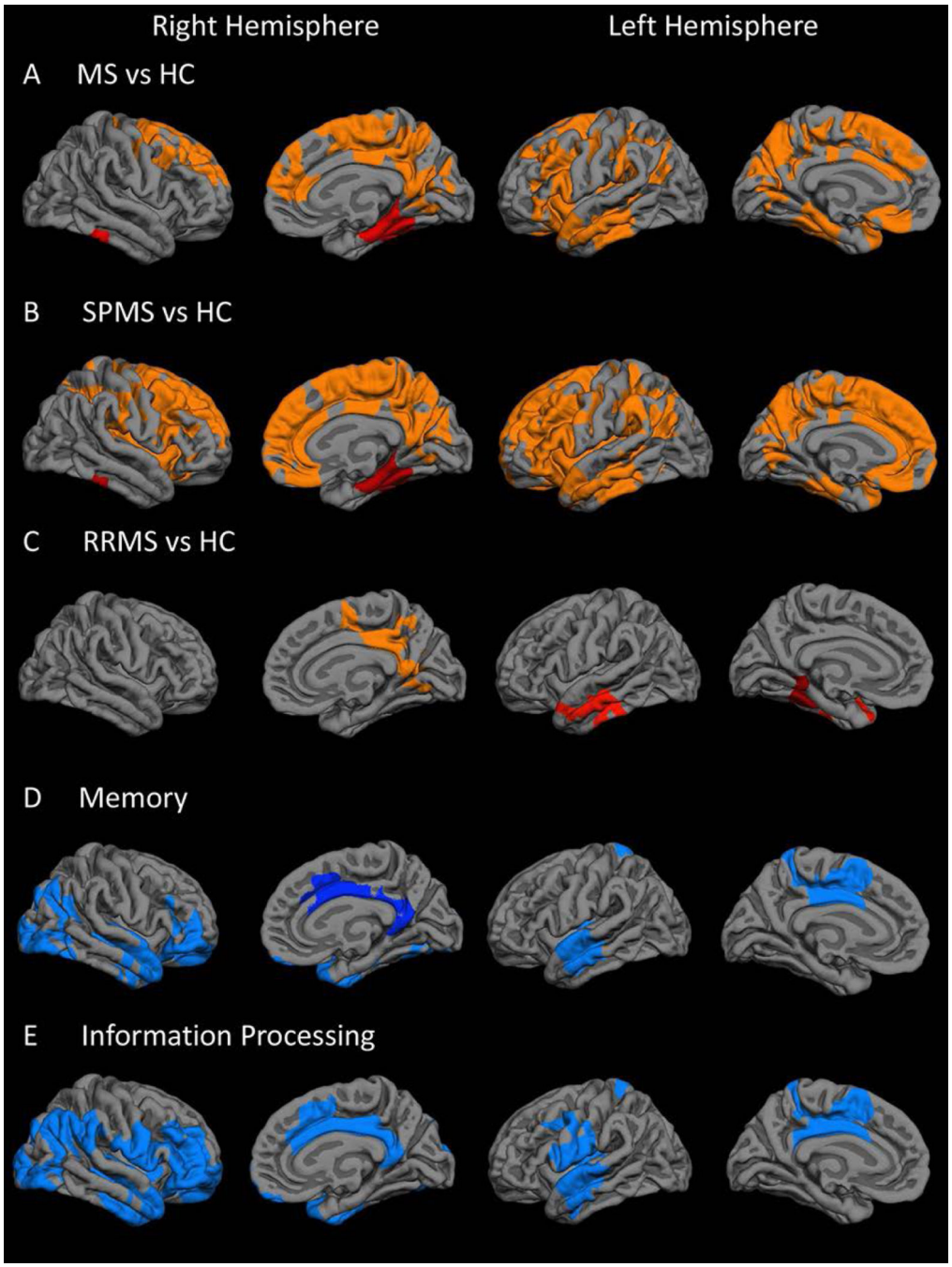

Figure 5.

Overlay of the general linear model significance maps ($p<0.05$, corrected for multiple comparisons, adjusting for age, binding genotype and cortical thickness) on the average pial surface showing, relative to healthy controls (HC, n=14), regions of increased ^{11}C-PBR28 normalized standardized uptake values (SUVR) **A)** in the whole multiple sclerosis (MS) cohort (n=27), as well as **B)** in the secondary-progressive MS (SPMS, n=15) and **C)** in the relapsing-remitting MS (RRMS, n=12) subgroups. Regions in all MS cases where ^{11}C-

PBR28 uptake correlated negatively ($p<0.05$, corrected for multiple comparisons) with **D)** memory and **E)** information processing speed function.

Table 1

Participants' demographics, clinical and MRI characteristics.

	Controls (n = 14)	All MS (n = 27)	SPMS (n = 15)	RRMS (n = 12)
Demographics and clinical data, mean (SD) or median [range]				
Gender (F/M)	6/8	21/6	11/4	10/2
Age, years	48 (13)	48 (10)	52 (7)	43 (10)
HAB/MAB	7/7	16/11	10/5	6/6
EDSS	-	4 [1-7.5]	6.5 [2-7.5]	2 [1-6]
SDMT	-	−0.4 (1.8)	−1.4 (1.4)	0.9 (1.3)
Information Processing	-	−0.9 (2.1)	−1.9 (1.9)	0.3 (1.8)
Executive Function	-	−1.3 (2.3)	−2.0 (2.6)	−0.3(1.5)
Learning Recall	-	−0.4 (1.3)	−0.70 (1.30)	−0.05 (1.2)
Disease duration, years	-	7 [1-21]	21 [6-40]	2 [1-33]
Subjects with at least 1 cognitive test z-scores ≤−1.5	-	20	13	7
Subjects with mild/moderate depression	-	3/4	2/2	1/2
MS Treatments				
Dimethyl fumarate	-	6	2	4
Natalizumab	-	5	3	2
Glatiramer acetate	-	4	2	2
Beta-Interferons	-	2	0	2
Rituximab	-	2	2	0
Fingolimod	-	1	1	0
Teriflunomide	-	1	0	1
None	-	6	5	1
MRI metrics, mean (SD) or median [range]				
WM lesion volume cm^3	-	8.1 (11.5)	12.6 (13.8)	2.6 (3.3)
Cortical thickness mm^2	2.39 (0.11)	2.33 (0.08)$^{\#}$	2.32 (0.10)$^{\#}$	2.36 (0.06)
Thalamic fraction$^{\wedge}$	$(6.1(0.9))10^{-3}$	$(5.5(1.1))10^{-3}$	$(5.2(0.9))10^{-3}$$^{\#}$	$(5.9(0.1))10^{-3}$
Hippocampal fraction$^{\wedge}$	$(2.8(0.6))10^{-3}$	$(2.7(0.7))10^{-3}$	$(2.5(0.6))10^{-3}$	$(2.9(0.8))10^{-3}$
Intracortical lesions, n	-	10 [2-69]	20 [3-69]	5 [2-32]
Leukocortical lesions, n	-	4 [1-151]	4 [1-151]	5 [1-7]
All cortical lesions, n	-	13 [1-171]	16 [1-171]	8 [3-39]

MS= multiple sclerosis; RRMS= relapsing-remitting MS; SPMS= secondary-progressive MS; SD= standard deviation; HAB= high affinity binders; MAB= mixed affinity binders; EDSS= Expanded Disability Status Scale; SDMT= Symbol Digit Modalities Test, WM= white matter; n= number.

*Beck Depression Inventory-II scores for mild depression= [14-19]; for moderate depression= [20-28]

$^{\wedge}$thalamic or hippocampal volume / total intracranial volume

$^{\#}$p<0.05 by Mann-Whitney-U-test

Table 2

Corrected p-values, effect size (Cohen's *d*) and standard errors for comparisons by linear regression (covarying for age and binding affinity) of ^{11}C-PBR28 uptake across different brain tissue compartments in MS subjects vs controls.

	MS vs Controls			SPMS vs Controls			RRMS vs Controls		
	p-value	***ES****	***SE***	***p-value***	***ES****	***SE***	***p-value***	***ES****	***SE***
SUVR	(n = 27 vs 14)			(n = 15 vs 14)			(n = 12 vs 14)		
Cortex	0.007	0.9	0.06	0.01	1.3	0.08	0.1	0.8	0.07
NAWM	0.02	0.9	0.07	0.01	1.3	0.08	0.5	0.5	0.07
WML	0.4	0.3	0.07	0.2	0.6	0.08	0.9	0.1	0.07
ICL	0.007	1.4	0.06	0.01	1.6	0.09	0.04	1.4	0.08
LCL	0.02	1.1	0.07	0.02	1.2	0.08	0.1	1.1	0.1
Thal	0.008	1.2	0.1	0.002	1.7	0.2	0.3	0.9	0.1
Hipp	0.006	1.3	0.06	0.003	1.6	0.09	0.1	1.1	0.07
BG	0.02	1.0	0.06	0.01	1.3	0.09	0.3	0.8	0.07
DVR	(n = 15 vs 11)			(n = 10 vs 11)			(n = 5 vs 11)		
Cortex	0.0007	1.5	0.07	0.005	1.7	0.09	0.03	1.5	0.07
NAWM	0.001	1.5	0.07	0.004	1.6	0.09	0.1	1.3	0.09
WML	0.05	0.9	0.07	0.05	1.1	0.08	1	0.3	0.06
CL[#]	0.02	1.5	0.1	0,03	3.1	0.1	0.03	1.5	0.07
Thal	0.005	1.3	0.1	0.004	1.9	0.1	0.7	0.8	0.1
Hipp	0.04	1.1	0.1	0.05	1.2	0.1	1	0.8	0.07
BG	0.02	1.1	0.07	0.02	1.4	0.07	0.9	0.5	0.06

MS= multiple sclerosis; RRMS= relapsing-remitting MS; SPMS= secondary-progressive MS; normal appearing white matter (NAWM); WML= white matter lesions; ES= effect size; SE= standard error; ICL= intracortical lesions; LCL= leukocortical lesions; CL= cortical lesions; Thal= thalamus; Hipp= hippocampus; BG= basal ganglia; SUVR normalized standardized uptake values; DVR= normalized volume of distribution ratios.

[*] The effect size was computed by adjusting the calculation of the pooled standard deviation with weights for the sample size.

[#] SPMS, n = 6; RRMS, n = 3.

Table 3

FreeSurfer surface-based analysis of cortical ^{11}C-PBR28 SUVR.

	Hemisphere	Surface Area (mm^2)	Corrected p-value	Area of peak p-value for between-group differences
All MS vs. Controls	Right	2,444	0.002	Parahippocampal
		16,281	0.0001	Precuneus
		1,602	0.04	Superior Parietal
		1,772	0.02	Lateral Orbitofrontal
	Left	33,578	0.0001	Supramarginal
RRMS vs. Controls	Right	3,707	0.000	Pericalcarine
	Left	1,725	0.009	Fusiform
		2,362	0.001	Inferior Temporal
SPMS vs. Controls	Right	1,725	0.009	Fusiform
		2,362	0.001	Inferior Temporal
	Left	47,009	0.000	Postcentral

	Hemisphere	Surface Area (mm^2)	Corrected p-value	Area of peak p-value for correlation with cognitive scores
Memory (CVLT-II – BVMT-R)	Right	2,406	0.001	Isthmus Cingulate
		5,131	0.0001	Temporal Pole
		4,444	0.0001	Lateral Orbitofrontal
		6,360	0.0001	Lateral Occipital
	Left	3,597	0.0001	Paracentral
		3,059	0.0001	Superior Temporal
Information Processing (SDMT – Trails A)	Right	14,902	0.0001	Inferior Parietal
		3,507	0.0001	Posterior Cingulate
		10,460	0.0001	Precentral
		6,888	0.0001	Superior Temporal
	Left	3,904	0.0001	Superior Frontal

SUVR= normalized standardized uptake values; MS= multiple sclerosis; RRMS= relapsing-remitting MS; SPMS= secondary-progressive MS; CVLT-II= California Verbal Learning Test-II; BVMT-R= Brief Visuospatial Memory Test–Revised; SDMT= Symbol Digit Modalities Test; Trails= Trails Making Test.